Scientia Iranica (2024) 31(4), 295–309

Sharif University of Technology
Scientia Iranica
Transactions B: Mechanical Engineering
https://scientiairanica.sharif.edu

Hyperelastic and viscoelastic modeling of the ovine intervertebral disc tissue

B. Jafari, V. Shams Esfand Abadi, and S. Sadeghnejad*

Bio-Inspired System Design Laboratory, Department of Biomedical Engineering, Amirkabir University of Technology (Tehran Polytechnic), Tehran, P.O. Box 1591634311, Iran.

Received 9 July 2021; received in revised form 17 August 2022; accepted 5 April 2023

KEYWORDS
Intervertebral Disc (IVD) tissue;
Viscoelastic;
Hyperelastic;
Linear;
Nonlinear;
Constitutive models;
Uniaxial compression.

Abstract. The Intervertebral Disc (IVD) carries compressive loads and resists the tensile and shear stress produced during bending and rotational movements. Hence, identifying its mechanical behavior has always encouraged researchers to propose various models for this tissue. Both viscoelastic and hyperelastic behavior have been observed regarding IVD. Therefore, this study aims to mechanically characterize the tissue using the existing hyperelastic and viscoelastic constitutive models and further discusses the best ones. Three stress relaxation tests were performed on ten ovine cervical IVD samples to evaluate their viscoelastic behavior. Models with linear, quasi-linear, and nonlinear behavior were implemented. For the hyperelastic response, another test was carried out using a load with a constant strain rate to fit seven previously suggested hyperelastic constitutive models to our recorded data. All tests were performed as uniaxial compression. Calculations were made using isotropy and incompressibility assumptions. Results approved the nonlinearity of the tissue's viscoelastic behavior since the linear models predicted divergent responses for different strain inputs. However, modified superposition theory, featuring a time- and strain-dependent relaxation function, was the most accurate model to predict the IVD response at different strain levels. As for hyperelasticity, Mooney-Rivlin, Yeoh, and Veronda-Westmann models fitted the experimental data with higher R^2 values.

1. Introduction

Intervertebral Discs (IVDs) act as shock absorbers between the vertebral bodies in the spinal column and permit the movements of the spine due to their capability of tolerating both axial and shear forces. The mechanical function of this tissue is highly related to its structure, which consists of two main parts: (a) A thick Annulus Fibrosus (AF) on the outer layers of the disc and (b) Nucleus Pulposus (NP), which is in the center of the disc structure. The semi-

*. *Corresponding author. Tel.: +98 21 64545952; Fax: +98 21 66468186*
E-mail addresses: bahram.jafari@aut.ac.ir (B. Jafari); shams.es@aut.ac.ir (V. Shams Esfand Abadi); s.sadeghnejad@aut.ac.ir (S. Sadeghnejad)

To cite this article:
B. Jafari, V. Shams Esfand Abadi and S. Sadeghnejad, "Hyper and viscoelastic modeling of the ovine intervertebral disc tissue", *Scientia Iranica* (2024) **31**(4), pp. 295-309
DOI: 10.24200/sci.2023.58687.5849

fluid structure of the NP is formed of a gelatinous substance, while the AF is like a cover of collagen fiber networks with an onion-like structure trapping the fluid inside [1].

The review of literature is categorized into three groups. First comes a short review of the selection of the animal samples. Then, the following two paragraphs review the related literature about hyperelastic and viscoelastic modeling, respectively. In order to improve the designs in the field of orthoses and orthopedics, theoretical models of tissues are needed for numerical simulations, which necessitate mechanical characterization [2–4]. For mechanically characterizing the IVD, a proper sample should first be selected. As for in vitro experiments, human specimens are more accurate to use than animal samples. However, there are several challenges in using human specimens, such as the difficulty in finding fresh human specimens, specifically from the young population. Moreover, there is a considerable variation in the mechanical properties and geometry of the human samples due to differences in gender, age, bone quality, and disc degenerative changes [5]. Furthermore, in research studies, using animal samples instead of human ones is more time- and cost-efficient and is still considered a preliminary effort toward human tissue characterization [6]. Despite the intrinsic limitations and simplifications of this substituting method, animal samples are more readily available and have more uniform geometries. Among the options, sheep are considered a preferred choice because of the many similarities in their disc anatomy with humans [5]. Sheep have a vertebral body, cross-sectional area, and spinal canal size similar to those of humans, as well as analogous IVD structural geometry. In research to see whether the sheep spine is a reliable model for human spine studies, Kandziora et al. [7] concluded that the ovine motion segment C3-C4 was the most suitable sample for the human motion segment. Most in-vitro studies have chosen the human age range of 20–55 for their investigations on the biomechanics of IVD [7,8].

Several studies assumed isotropic and linear elastic behavior for the IVD components in compression and tension [9–11]. Elastic models were primarily implemented for short-term responses or dynamic investigations. Martins et al. [12], using numerous experimental data and theoretical models from the literature, performed a comparison on the mechanical behavior of the IVD and concluded that hyperelastic models are better at describing the tissue compared to the linear elastic ones. They compared seven hyperelastic models and found that Yeoh and Ogden's models resulted in the best correlation with experimental data. Their comparison was performed on silicone-rubber and pig muscular tissue. Hyperelastic models have been extensively used to model the IVD tissue and its constituents [1,13,14] for various reasons, such as identifying the tissue properties under fast dynamic compressive load [13], predicting mechanical failures using finite element simulation method [6], and investigating the short-term response and strain rate dependency of the IVD's mechanical behavior [14]. Ghezelbash et al. [1] employed hyperelastic models for the IVD to predict the failure threshold of AF in different directions. Recently, Yahyaiee et al. [15] compared several hyperelastic models for the IVD under physiological loads. Their results suggested that the Yeoh model had the best consistency with the experimental data.

On the other hand, numerous researchers have suggested viscoelastic models for IVD to describe its time-dependent response [16–18]. Ekström et al. [17] implemented three-parameter and four-parameter linear viscoelastic models for the entire IVD tissue to investigate the creep behavior and the time-dependent response of the tissue in cyclic compressive loading. However, they declared that the parameters they obtained were dependent on the load magnitude and could barely be compared to the parameters achieved by different input loads, which was due to the nonlinear viscoelasticity of the tissue. Ellingson and Nuckley [18] performed stress relaxation tests up to 15% strain level to spatially characterize the viscoelastic parameters of the IVD tissue. They used the Prony (PRO) series for the stress relaxation function of the linear model, which yielded a time-dependent viscoelastic response. Groth and Granata [19] introduced a nonlinear model to modify the standard linear solid one. They stated that the parameters of linear models were strain-independent and could not explain the nonlinear behavior of the IVD tissue. Quasi-Linear Viscoelastic (QLV) models can also be employed for the IVD, the stress relaxation functions of which assigned separated functions for time and strain dependencies [20]. Therefore, the time-dependent part was not a function of strain level, and the same rate of relaxation was predicted for all strain levels. However, the behavior of soft tissues can deviate from the QLV assumption. Thus, fully nonlinear models such as the Modified Superposition (MSP) theory, using interconnected constitutive coefficients, have previously been proposed to phenomenologically model the nonlinear viscoelastic behavior in a general but more accurate way [21]. The nonlinear superposition method has also been used to describe the nonlinear viscoelasticity of soft tissues such as ligaments, smooth muscle, connective and cartilaginous tissue [16,22]. Sciortino et al. [23] used a new method based on fractional calculus to fully model the viscoelastic behavior of the IVD. Recently, Jafari et al. [24] employed a nonlinear viscoelastic model for the IVD to capture its time- and displacement-dependent behavior and link the tissue model with a haptic simulation algorithm.

However, there was no trace of using MSP theory for predicting the nonlinear viscoelastic response of the IVD in the recent literature.

In order to clarify the need and necessity of this study, it must be summarized that linear viscoelastic models can be used to predict tissues' behavior in different strain levels (in stress relaxation tests), provided that the tissue behaves linearly viscoelastic entirely. Otherwise, nonlinear models must be employed. However, if the nonlinearity of the tissue is not prominent to a great extent, as a simpler approach for modeling, the quasi-linear formulation can be used instead of a completely nonlinear (and inseparable) one. Hence, the predictability of viscoelastic models should be assessed for the tissues under the study. Although there have been many studies in the literature characterizing the mechanical behavior of the IVD, there is still a need for a fair and comprehensive comparison between the viscoelastic models for the IVD tissue in terms of and focusing on their viscoelastic linearity behavior. In addition, among those who were not interested in considering the viscoelastic behavior of the IVD, very few researchers compared a sufficiently wide variety of hyperelastic models for the tissue under uniaxial compression. Consequently, the parameters of these models have not been investigated thoroughly, while these comparisons and identified parameters add to what is already known in this field and can be assistive in future modeling and simulations of this tissue. Consequent to the mentioned needs, the primary purpose of this study is to characterize the general mechanical properties of the ovine IVD tissue under uniaxial compressive load based on the existing hyperelastic and viscoelastic constitutive models and select the best one in terms of the closeness of each model's prediction to our experimental data. The nonlinearity of the viscoelastic behavior of the IVD will also be discussed.

At the beginning of Section 2, our general method for achieving the aforementioned purpose is briefly expressed, which includes stress relaxation tests and a compressive test with a constant strain rate. The first part of this section provides details about the preparation of the IVD samples used in this study, while the second part describes the experimental setup and each mechanical test performed. Next comes the elaboration of the theory of three common viscoelastic models, showing linear, quasi-linear, and nonlinear viscoelastic behavior, respectively. Finally, the last part deals with the continuum-based formulation required for deriving hyperelastic constitutive models from the strain energy functions suggested by the literature. In Section 3, the results of hyperelastic and viscoelastic modeling are presented and discussed. Finally, concluding comments are delivered in Section 4, to sum up the entire manuscript.

2. Materials and methods

In this study, stress relaxation tests with three different constant displacements were performed on ten ovine cervical IVD samples to assess the viscoelastic behavior of the tissue. Displacements were applied as uniaxial compression, ultimately providing the stress- and strain-time data for each sample. The stress and strain data of the samples were averaged for each time point, and the mean values were expressed and used here. First, isochronal tests were performed on the data to determine the linear or nonlinear viscoelastic behavior of the tissue under the tests' conditions. Then, three viscoelastic constitutive models, namely, the linear viscoelasticity (using two forms of the PRO series), the QLV formulation, and the MSP theory of nonlinear viscoelasticity, were fitted to the experimental data to obtain the models' parameters and further evaluate each model's predictability at different strain levels. Furthermore, a compressive load with a constant strain rate was applied to the samples, and the mean Cauchy stress values against their corresponding strain data were achieved. Seven hyperelastic constitutive models were fitted to the mean data from the samples to select the best fitting one. All curve fitting procedures were executed by MATLAB curve fitting toolbox, using the Levenberg-Marquardt algorithm.

2.1. IVD sample preparation

Ten fresh ovine IVD samples from the entire fourth cervical (C4) motion segments were obtained from an abattoir. The specimens included healthy discs attached to their two vertebral bodies and endplates. The samples were stored at $-17°C$ during the isolation time and then kept in physiological saline solution at ambient temperature for 5 hours prior to the test to make sure the tissue retained the mechanical properties of its physiological condition. Soft tissues, posterior processes, and other elements were removed from the samples, but the vertebral bodies and the endplates were not detached from the rest of each sample, leaving a VB-disc-VB specimen for each one, which is a conventional method in uniaxial compressive disc characterizations [25]. Since the covering vertebral plates are significantly stiffer compared to the IVD [18], and the applied loads are too small to bring about any deformation or fracture of the plates, the vertebral plates are considered rigid, and thus, the recorded force and displacement data are produced merely as a result of the IVD's deformation. In addition, to ensure exerting a pure axial compression, the top and bottom surfaces of the sectioned vertebral bodies were carefully placed and fixed parallel to the disc and the horizontal planes by which the disc is reinforced, as suggested by the literature [10]. The geometrical properties, including the samples' initial lengths and their cross-

sectional areas, were precisely measured before each test using digital photography and computer imaging (Figure 1(a)). Dimension calculations were carried out using the sketch picture tools in SolidWorks 2017. The initial lengths and cross-sectional areas of the samples were calculated to be 5.02 ± 1.43 mm and 389.41 ± 81.37 mm^2, respectively.

2.2. Experimental setup and mechanical tests

All tests were carried out at room temperature by a dynamic testing machine (Hct400/25), equipped with a load cell having the least sensitivity of 0.0001 N, Zwick Roell Group, Ulm, Germany (Figure 1(b)). Before performing the tests, five loading and unloading cycles (up to 4% strain amplitude with a frequency of 1.0 Hz) were applied to the samples as the preconditioning phase to obtain reproducible results in the relaxation tests and ensure the evaluation of the correct tissue's characteristics. Also, the samples were kept wet by spraying a physiological saline solution to prevent tissue dehydration, which otherwise could cause the samples' properties to change during the tests [25]. Additionally, the samples were set to rest in the saline solution between each test for a duration sufficiently longer than their relaxation time to recover their initial configuration.

In all tests, compressive and uniaxial initial loads or displacements were applied. The relaxation set of tests included three tests, either of which was initiated by a constant displacement, thus starting with three constant strain values (the inputs). The strain amplitudes were set to be 4%, 8%, and 16%. Load response data were obtained during the tissue relaxation period for an aggregate number of 10000 data points in 300 seconds. It is noteworthy that since it is physically impossible to apply the relaxation input as a unit step function, a rise-time at the beginning of data will always exist due to the impact nature of the input strain. Since the rise-time contradicts the assumptions on which the analytical calculations are based, it may produce some errors. Therefore, to diminish such effects, as a common method suggested by the literature [16], the analysis was performed on the data starting at a point ten times longer than the rise-time period. In the relaxation tests, the response data were force versus time points. The cross-sectional areas of the samples were used to determine the engineering stress for each sample. Finally, the stress values were averaged at each time point, and the obtained "mean stress versus time" data were fitted by viscoelastic models.

In addition to the relaxation tests, uniaxial compression with the constant strain rate of 4% s^{-1} was exerted on the samples up to 600 N to study the hyperelastic response of the IVD tissue based on the available constitutive models. According to Kasra et al. [26], the value of the strain rate in our experiment is considered medium. Hence, it was low enough to preclude impact loading. Therefore, it can successfully capture and characterize the hyperelastic behavior of the tissue. The geometrical measurements of each sample at the beginning of the tests, along with the incompressibility assumption for the IVD samples, made it possible to calculate the "mean Cauchy stress versus mean stretch" data from the load-displacement records.

2.3. Viscoelastic modeling and formulations

We undertook a simple nonlinearity assessment using an isochronal test beforehand. For doing this, the mean stress-strain data were selected at ten different time points. If a linear function fits the data well, the acceptability of the linearity assumption will be confirmed.

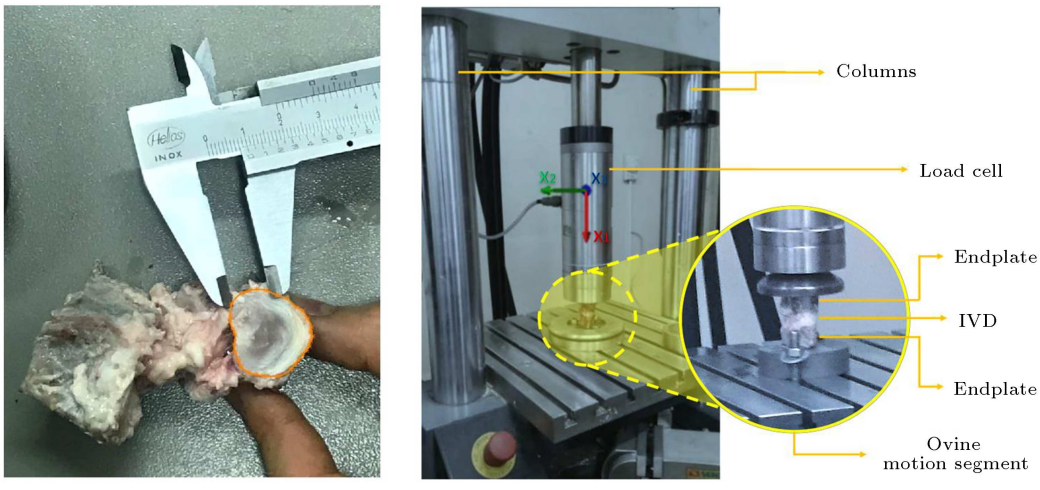

Figure 1. (a) Measuring initial length and cross-sectional area of a sample. (b) A sample placed in the testing machine.

Table 1. Stress functions of the viscoelastic models used in this study.

Viscoelastic model	Status	Stress function
Two-term Prony (PRO) model	Linear	$\sigma(t) = \varepsilon_0(E_0 + E_1 e^{\frac{-t}{\tau_1}})$
Three-term Prony (PRO) model	Linear	$\sigma(t) = \varepsilon_0(E_0 + E_1 e^{\frac{-t}{\tau_1}} + E_2 e^{\frac{-t}{\tau_2}})$
Fung's Quasi-Linear Viscoelastic (QLV) model	Partly linear	$\sigma(\varepsilon, t) = \varepsilon_0 G(\varepsilon) t^n$
Modified Superposition (MSP) model	Nonlinear	$\sigma(\varepsilon, t) = \varepsilon_0 A(\varepsilon) t^{B(\varepsilon)}$

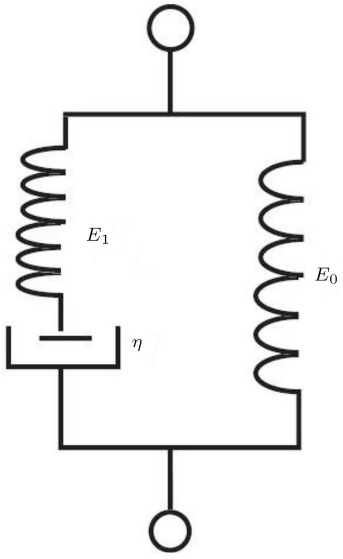

Figure 2. Standard linear solid model [21].

2.3.1. Linear viscoelastic models

As an introduction to linear viscoelasticity, the standard linear solid model with three parameters, illustrated in Figure 2, was selected [21], by which the necessary formulations were derived. Using the standard linear solid configuration, the following differential equation was obtained:

$$\frac{d\sigma}{dt} + \frac{\sigma}{\tau} = \frac{d\varepsilon}{dt}(E_0 + E_1) + \frac{\varepsilon E_0}{\tau}. \quad (1)$$

Linear viscoelastic modeling is generally based on Boltzmann superposition integral, which can be written in the relaxation form as the following [21]:

$$\sigma(t) = \int_0^t E(t-\tau)\frac{d\varepsilon(\tau)}{d\tau}d\tau, \quad (2)$$

where E(t) denotes the relaxation function, σ(t) is the stress response as a function of time, ε refers to the strain, and τ is the integration variable.

Using the Boltzmann superposition integral, differential Eq. (1) is solved and leads to the relaxation function for the standard linear solid, which is found to be a decreasing exponential as the following:

$$E(t) = E_0 + E_1 e^{\frac{-t}{\tau_r}}, \quad (3)$$

where τ_r is known as the relaxation time and is equal to η/E_1. Another way to achieve the relaxation function for linear viscoelastic modeling in a more general sense is by employing a PRO exponential series. As for the relaxation function, the PRO series formulation results in the following:

$$E(t) = E_0 + \sum_{i=1}^{n} E_i e^{\frac{-t}{\tau_i}}. \quad (4)$$

We assumed a step function for the strain input ($\varepsilon(t) = 0$ if $t = 0$ and $\varepsilon(t) = \varepsilon_0$ if $t > 0$). To implementing the PRO series, we got the following equation for the linear viscoelasticity:

$$\sigma(t) = \varepsilon_0 \left(E_0 + \sum_{i=1}^{n} E_i e^{\frac{-t}{\tau_i}} \right). \quad (5)$$

The parameters of this model are E_0, E_i, and τ_i, which will be achieved by fitting this equation to the stress relaxation data corresponding to each strain level. Two- and three-term PRO series were used, and the associated equations were listed in Table 1.

The Linear viscoelasticity assumption does not allow any changes in the model parameters for different strain levels. Thus, in order to evaluate the predictability of this model for the tissue, Eq. (5) was used to fit the relaxation data from the average strain level. Hence, the results gave the model parameters at the average strain level. The obtained parameters were held constant and used to fit Eq. (5) to each set of relaxation data (from other strain levels) so as to quantify the deviation of this model at each strain level from the linearity assumption.

2.3.2. QLV theory

The theory of QLV was proposed by Fung [27], the advantage of which is that the relaxation function depends on strain as well as time. The separable relaxation function ($E(\varepsilon, t)$) can be written in the form below:

$$E(\varepsilon, t) = G(\varepsilon)T(t). \quad (6)$$

In Eq. (6), G and T are functions of strain and time, respectively. With such a relaxation function, one can reach the following integration:

$$\sigma(\varepsilon, t) = \int_0^t T(t-\tau) G(\varepsilon) \frac{d\sigma}{d\varepsilon} \frac{d\varepsilon(\tau)}{d\tau} d\tau. \quad (7)$$

Again, a step function for the input strain was selected and the following formulation for the stress was achieved:

$$\sigma(\varepsilon,t)=\varepsilon_0 G(\varepsilon)T(t). \tag{8}$$

In this model, we assumed ($T(t)=t^n$) in which n is a constant, known as the rate of relaxation [16]. Since $T(t)$ is only a function of time, the coefficient n does not depend on the strain, and hence, it remains constant at every stain level. This aids in evaluating the accuracy of the model's predictability in different strain levels.

2.3.3. MSP theory of nonlinear viscoelasticity

Similar to the QLV, the MSP theory proposes the relaxation function as a function of both time and strain. However, in this theory, the time and strain contributions are not separable. The following integration is presented by this model [22]:

$$\sigma(\varepsilon,t)=\int_0^t T(t-\tau,\varepsilon(\tau))\frac{d\varepsilon(\tau)}{d\tau}d\tau. \tag{9}$$

Using a power law, a formulation similar to the QLV one is introduced. However, unlike in the QLV, the exponent $B(\varepsilon)$ is a function of strain.

$$E(\varepsilon,t)=A(\varepsilon)t^{B(\varepsilon)}. \tag{10}$$

The following stress formulation is obtained by applying the strain input as a step function:

$$\sigma(\varepsilon,t)=\varepsilon_0 A(\varepsilon)t^{B(\varepsilon)}, \tag{11}$$

$A(\varepsilon)$ and $B(\varepsilon)$ are functions of strain and are determined using the isochronal data along with the stress relaxation data.

2.4. Hyperelastic modeling and formulations

The basic general measurement of the deformational motion of a continuum element is the deformation gradient. The material element dX at the reference configuration is mapped, by this motion, to the material element dx at the new configuration through the deformation gradient tensor, F.

$$dx=FdX. \tag{12}$$

Assuming the uniaxial load is applied in x_1 direction, the principal axes of deformation are the x_1 direction and the two perpendicular transverse directions (x_2 and x_3), shown in Figure 1(b).

$$dx_i=\lambda_i dX_i \qquad i=1,2,3, \tag{13}$$

where λ_1, λ_2, and λ_3 are the principal stretches in the x_1, x_2, and x_3 directions. We imposed the incompressibility condition ($\det(F)=J=\lambda_1\lambda_2\lambda_3=1$), which is reasonable, given that the NP holds a high bulk modulus with a semiliquid structure. This is the reason that the nucleus deforms laterally (instead of compressing its volume) when loaded under spinal vertical compressive forces. Additionally, the AF is a soft tissue with high water content. Thus, incompressibility was reported as a generally accepted assumption for the hyperelastic modeling of such soft tissues [12]. We also assumed the cross-sections of the samples (perpendicular to the x_1 direction) to be symmetric ($\lambda_2=\lambda_3$). Therefore, considering $\lambda_1=\lambda$, we get:

$$F=\begin{bmatrix}\lambda & 0 & 0\\ 0 & \lambda^{-\frac{1}{2}} & 0\\ 0 & 0 & \lambda^{-\frac{1}{2}}\end{bmatrix}. \tag{14}$$

Using Eq. (14), the right Cauchy-Green deformation tensor is defined below:

$$c=F^TF=\begin{bmatrix}\lambda^2 & 0 & 0\\ 0 & \lambda^{-1} & 0\\ 0 & 0 & \lambda^{-1}\end{bmatrix}. \tag{15}$$

Now, the invariants of the right Cauchy-Green deformation tensor are calculated as follows:

$$\begin{aligned}I_1&=tr(c)=\lambda^2+\frac{2}{\lambda},\\ I_2&=\frac{1}{2}\left((tr(c))^2-tr\left(c^2\right)\right)=2\lambda+\frac{1}{\lambda^2},\\ I_3&=1.\end{aligned} \tag{16}$$

These invariants and principal stretches are used to express the strain energy function in the case of isotropic hyperelastic materials. Therefore, the Cauchy stress expressions can be defined as a function of the strain invariants and the principal stretches. The choice of each approach generally depends on the form of the strain energy density function, W. For instance, the Cauchy stress expressions as a function of the principal stretches for incompressible materials given by Ogden [2] are as below:

$$\sigma_i=\lambda_i\frac{\partial W}{\partial\lambda_i}-p, \qquad i=1,2,3, \tag{17}$$

where p is the hydrostatic pressure and is determined by the boundary conditions. However, by the following subtraction, we get:

$$\sigma_1-\sigma_2=\lambda_1\frac{\partial W}{\partial\lambda_1}-\lambda_2\frac{\partial W}{\partial\lambda_2}. \tag{18}$$

Since our experiment was based on simple uniaxial compression tests ($\sigma_1=\sigma,\sigma_2=\sigma_3=0$), the following is obtained for the Cauchy stress dependency on the stretch values:

$$\sigma=\lambda_1\frac{\partial W}{\partial\lambda_1}-\lambda_2\frac{\partial W}{\partial\lambda_2}. \tag{19}$$

Below is another form of Cauchy stress, which is written using the strain invariants [12]. This equation can be derived from Eq. (19) using Eq. (16), the incompressibility assumption, and the uniaxial loading condition:

$$\sigma = 2\left(\lambda^2 - \frac{1}{\lambda}\right)\left(\frac{\partial W}{\partial I_1} + \frac{1}{\lambda}\frac{\partial W}{\partial I_2}\right). \tag{20}$$

In the last two equations, W is substituted by several expressions that were previously suggested in the literature. To make this approach more clear, one general form of the strain energy density function for hyperelastic materials, known as the Rivlin expression, is shown here by the following series [28].

$$W = \sum_{i,j,k=0}^{\infty} C_{ijk}(I_1 - 3)^i (I_2 - 3)^j (I_3 - 1)^k. \tag{21}$$

Note that $C_{000} = 0$ because the strain energy must be zero in the undeformed configuration. Also, recall that in the problem of incompressible materials, I_3=1. Therefore, keeping the first terms of the Rivlin expression, Eq. (22) is written as below:

$$W = C_{10}(I_1 - 3) + C_{01}(I_2 - 3). \tag{22}$$

The above equation is known as the Mooney-Rivlin model. Similarly, Table 2 presents a list of several strain energy density functions for incompressible and isotropic hyperelastic materials, which have been previously used for many biological cartilaginous and soft tissues in the literature [29,30].

Now, noting that our experiments were performed as uniaxial compression tests, the Cauchy stress for the Mooney-Rivlin model can be calculated using Eq. (20):

$$\sigma = 2\left(\lambda^2 - \frac{1}{\lambda}\right)\left(C_{10} + \frac{C_{01}}{\lambda}\right). \tag{23}$$

The same approach is applicable to other strain energy density functions in Table 2. By the use of Eqs. (19) and (20), the resultant Cauchy stress expressions of each strain energy density function were calculated for the uniaxial compressive test and listed in Table 3. Since our work involves the compression zone, the stress values must remain negative and be an increasing function of stretch [28].

3. Results and discussion

The results of this study were obtained based on considering the IVD tissue as a unit structure. In hyperelastic and viscoelastic modeling of the IVD, some authors have already considered the entire tissue as a homogenous and isotropic body. They reported material properties to characterize the tissue as a whole, using force-displacement or stress-strain graphs [10,17,19,24]. One reason for such simplification is the difficulty in modeling the fluid movement in the NP, AF, and between the two components when dividing up the disc. In addition, the orthotropic assumption will increase the material constants and complicate the viscoelastic analysis. Yang et al. [10] measured the homogenized "effective modulus" to characterize the

Table 2. Strain energy density expressions as a function of strain invariants and principal stretches.

Model	Strain energy density function
Mooney Rivlin	$W = C_1(I_1 - 3) + C_2(I_2 - 3)$
Neo-Hookean	$W = C_1(I_1 - 3)$
Fung	$W = \frac{C_1}{2C_2}(e^{C_2(I_1-3)} - 1)$
Yeoh	$W = C_1(I_1 - 3) + C_2(I_1 - 3)^2 + C_3(I_1 - 3)^3$
Ogden	$W = \frac{C_1}{C_2}(\lambda_1^{C_2} + \lambda_2^{C_2} + \lambda_3^{C_2} - 3) + \frac{C_3}{C_4}(\lambda_1^{C_4} + \lambda_2^{C_4} + \lambda_3^{C_4} - 3) + \frac{C_5}{C_6}(\lambda_1^{C_6} + \lambda_2^{C_6} + \lambda_3^{C_6} - 3)$
Humphrey	$W = C_1(e^{C_2(I_1-3)} - 1)$
Veronda-Westman	$W = C_1(e^{C_2(I_1-3)} - 1) - \frac{C_1C_2}{2}(I_2 - 3)$

Table 3. Cauchy stress formulation of the hyperelastic models as a function of strain invariants and principal stretches.

Model	Cauchy stress expression
Mooney-Rivlin	$\sigma = (\lambda^2 - \frac{1}{\lambda})(C_1 + \frac{C_2}{\lambda})$
Neo-Hookean	$\sigma = 2C_1(\lambda^2 - \frac{1}{\lambda})$
Fung	$\sigma = C_1(\lambda^2 - \frac{1}{\lambda})e^{C_2(I_1-3)}$
Yeoh	$\sigma = 2(\lambda^2 - \frac{1}{\lambda})(C_1 + 2C_2(I_1 - 3) + 3C_3(I_1 - 3)^2)$
Ogden	$\sigma = C_1(\lambda^{C_2} - \lambda^{-\frac{C_2}{2}}) + C_3(\lambda^{C_4} - \lambda^{-\frac{C_4}{2}}) + C_5(\lambda^{C_6} - \lambda^{-\frac{C_6}{2}})$
Humphrey	$\sigma = 2C_1C_2(\lambda^2 - \frac{1}{\lambda})e^{C_2(I_1-3)}$
Veronda-Westmann	$\sigma = 2C_1C_2(\lambda^2 - \frac{1}{\lambda})(e^{C_2(I_1-3)} - \frac{1}{2\lambda})$

average mechanical behavior of the disc tissue as a whole. Such simplifications greatly aid in the analysis, especially in studies with a large number of models being examined, such as in our work. The results can help obtain the stress or displacement profiles through the entire IVD structure and simplify the numerical use of the tissue's behavior in large-scale finite element simulations of a motion segment or the whole vertebral column in static and dynamic analyses.

3.1. Viscoelastic modeling results

Having the geometrical properties of the samples, the mean engineering stress and strain values were calculated from the force and displacement recorded data. The mean stress values against the relaxation time were plotted for each strain level in Figure 3(a). The overall profile of the relaxation plots with our three strain levels correlated well with the three relaxation plots in the study of Ellingson and Nuckley [18] (Figure 3(b)). The general shape of the plots also had a good consistency with those in the literature performing the same tests on other viscoelastic biological soft tissues [5,16].

To assess the level of linearity of the viscoelastic behavior of the IVD tissue, mean isochronal stress-strain data were achieved at ten different time points. The time points were (5.5, 12, 20, 30, 60, 100, 150, 180, 210, and 270 s). None of the mean stress-strain data of these time points could be fitted by a straight line, as can be seen in Figure 4. However, R^2 values were 1.00 for all the nonlinear polynomial functions fitted to the data (results not shown here). The mentioned findings indicated that if the strain level is changed, the stress response cannot be predicted by a linear function. Hence, the nonlinear viscoelasticity behavior of the IVD tissue was substantiated.

3.1.1. Linear viscoelasticity results

Two- and three-term PRO series were used to model the viscoelastic behavior of the IVD roughly. First,

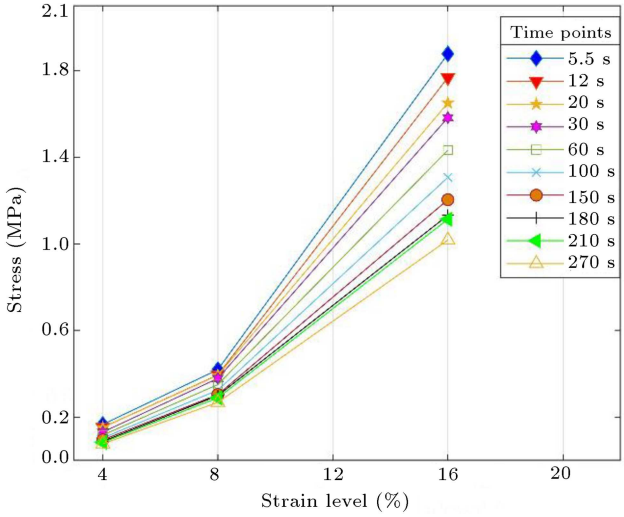

Figure 4. Mean isochronal stress-strain data at ten different time points.

Eq. (5) was fitted to each set of experimental data separately. These measures were taken for both two- and three-term PRO models. Tables 4 and 5 list the obtained parameters of each linear model and the R^2 values for different strain levels. Afterward, only the parameters obtained from the average strain level (9.3%) were used to make the main linear constitutive expression for relaxation, which is used to evaluate the predictability of the linear viscoelasticity assumption. To do this, the main constitutive expression, which is obtained using the parameters from the average strain data (9.3%), was fitted to the relaxation data corresponding to each strain level separately. The deviation of this model from the experimental relaxation data at each strain level was presented by the standard deviation parameter, which was then used to calculate the coefficient of determination, R^2.

According to Tables 4 and 5, both PRO models could fit the experimental data with high R^2 values for all the stain levels. Therefore, the linear viscoelastic

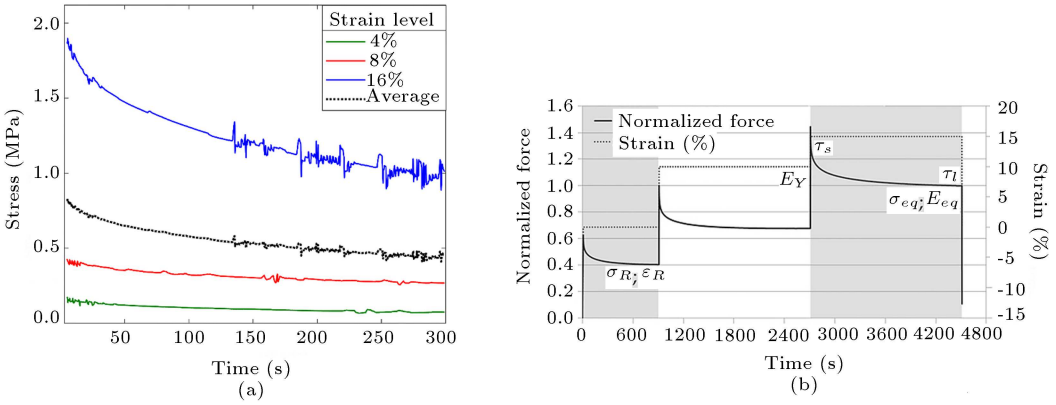

Figure 3. (a) The mean stress data versus the relaxation time at each strain level in this study. (b) Stress relaxation results at three strain levels in the study of Ellingson and Nuckley [18].

Table 4. Obtained parameters of the three-term PRO model at different strain levels.

Strain level (%)	E_0 (MPa)	E_1 (MPa)	E_2 (MPa)	τ_1 (s)	τ_2 (s)	R^2
4	1.328	2.058	0.6617	206.9	24.2	0.9702
8	2.342	2.14	0.7773	390.7	42.65	0.9826
16	5.184	5.266	2.02	176.9	14.45	0.9818
Average (= 9.3)	3.944	1.346	3.843	17.75	188.5	0.9886

Table 5. Obtained parameters of the two-term PRO model at different strain levels.

Strain level (%)	E_0 (MPa)	E_1 (MPa)	τ_1 (s)	R^2
4	1.676	2.116	122.3	0.9658
8	3.198	1.92	129.3	0.9792
16	5.847	5.412	117.5	0.9749
Average (= 9.3)	4.495	3.942	119.4	0.9826

model successfully captures the time dependency of the IVD's mechanical response at each strain level separately. However, the three-term PRO model produced a slightly better fit due to the higher number of coefficients. Besides, it should be noted that the first parameter of each model, which is E_0 and represents the largest share of elasticity, was increased with the strain level. More generally speaking, the sum of elastic parameters, E_i, increased by growing the strain level. This is because at $t = 0$, the parameters controlling the viscosity effect act as rigid elements. Hence, it allows the elements of elasticity to be proportional to the initial strain.

The parameters of both PRO models did not remain constant when the strain level was changed. This demonstrated the dependency of such parameters on the strain level and approved the insufficiency of the linear viscoelasticity assumption for the IVD tissue, as was shown in the nonlinearity assessment using the isochronal data. Therefore, consistent with the findings of Groth and Granata [19], for capturing the IVD's phenomenological behavior, nonlinear models should be used.

3.1.2. QLV model

A QLV model was applied to the mean experimental relaxation data of the IVD samples. Table 6 shows the calculated parameters of this model at each strain level. The parameter n was obtained for different values of each strain level. Therefore, this parameter was taken from the average strain level data (9.3%) and applied to the main QLV constitutive expression, which was used to quantify the deviation of this model from the corresponding set of experimental data at other strain levels. This method was described by previous studies to assess the model's predictability [16]. This approach is also equivalent to what we used for the linear viscoelastic model to obtain its predictability in other strain levels. The results of the QLV model are also listed in Table 7 for comparison with other models and plotted in Figures 5 and 6.

Table 6. Obtained parameters of the QLV model at different strain levels.

Strain level (%)	$G(\varepsilon)$	n	R^2
4	6.495	−0.2081	0.912
8	7.083	−0.1248	0.935
16	17.67	−0.1751	0.9398
Average (= 9.3)	13.01	−0.1679	0.945

3.1.3. MSP theory

Finally, the MSP theory was used as a nonlinear model of the IVD tissue. The parameters of the MSP model were found by fitting Eq. (11) to the experimental relaxation data at each strain level. The results are

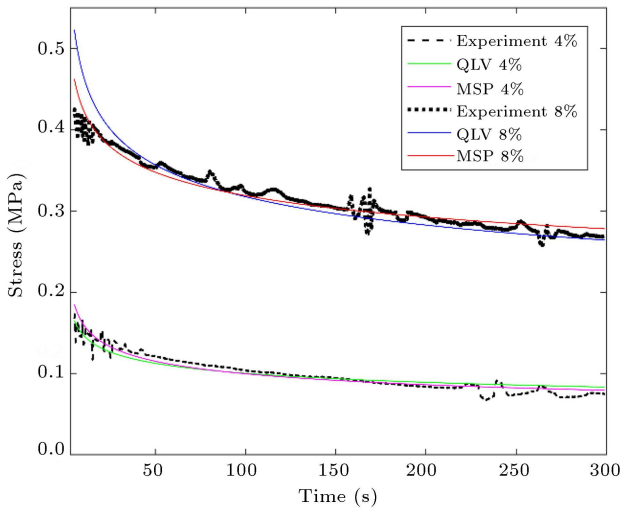

Figure 5. Predicted response of the QLV and the MSP models with the mean experimental data by 4% and 8% strain inputs.

Table 7. Obtained strain-dependent parameters and R^2 values of each viscoelastic model at different strain levels.

Strain level (%)	Model	Obtained strain dependent parameters	R^2
4	Two-term PRO	–	−44.0905
	Three-term PRO	–	−44.1143
	QLV	$G = 5.428$	0.8717
	MSP	$G = 6.495$ $n = -0.2081$	0.9121
8	Two-term PRO	–	−18.2065
	Three-term PRO	–	−18.2311
	QLV	$G = 8.6$	0.8034
	MSP	$G = 7.083$ $n = -0.1248$	0.9352
16	Two-term PRO	–	−1.0434
	Three-term PRO	–	−1.0355
	QLV	$G = 17.11$	0.9379
	MSP	$G = 17.67$ $n = -0.1751$	0.9398

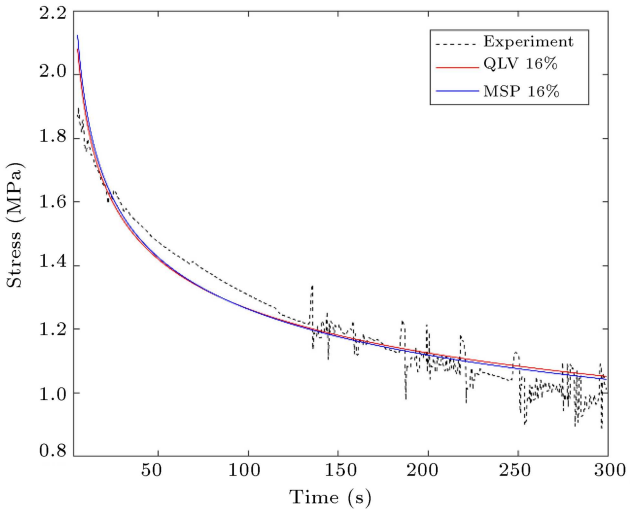

Figure 6. Predicted response of the QLV and the MSP models with the mean experimental data by 16% strain input.

not listed here because the obtained parameters were identical to those of the QLV model at the matching strain levels (see Table 6). However, one could not change the exponent, n, at different strain levels in the QLV expression. This inherent feature of the QLV model disabled this model to predict the tissue's accurate response at different strain levels. However, in the MSP model, both parameters were strain-dependent and able to change with the strain level. Therefore, we assigned second-order polynomials, suggested by the literature [16], in Eq. (11) for $A(\varepsilon)$ and $B(\varepsilon)$ to predict the parameter's dependency on the strain level. Implementing the three relaxation sets of the mean stress-strain data, A and B were found to be: $A(\varepsilon) = 980.3\varepsilon^2 - 102.9\varepsilon + 9.044$ and $(\varepsilon) = -22.59\varepsilon^2 + 4.794\varepsilon - 0.3637$ in which R^2 values were 1.00. The accuracy of this model's prediction at different strain levels is presented by R^2 values listed in Table 7. Additionally, Table 7 lists the predicted parameters by this method for all the viscoelastic models used in this study. According to Table 7, the MSP model was the most accurate one to obtain the tissue's response at different strain levels. This is due to its ability to take into account a relaxation function that is both time- and strain-dependent. Also, the predictability of this model seemed to be improving when the strain level was increased. On the other hand, the QLV model gave lower R^2 values as it predicted the same relaxation rate parameter, n, for all strain levels. It is also notable that the QLV's best prediction was at the strain level of 16%, where its constant parameter, n, was very close to the same parameter predicted by the MSP model at the 16% strain level. The quality of curve fitting can be observed in Figures 5 and 6. The least reliable prediction was for the PRO models in which no differences in the responses between the various strain inputs were reflected by the parameters. Negative R^2 values in Table 7 mean that the linear models did not follow the trend of the experimental data of other strain levels, even though the models'

constant parameters were obtained by the mean data from the average strain level. This proves the fact that the viscoelastic behavior of the IVD tissue is nonlinear, and the parameters obtained from the linear models cannot be used to describe this tissue in relaxation tests at other strain levels.

3.2. Hyperelastic modeling results

Uniaxial compressive load with the constant strain rate of 4% s^{-1} was carried out on the IVD samples to characterize the hyperelastic behavior of the tissue. Figure 7 shows the mean stress-stretch plot resulting from the force-displacement recorded data. It is evident from the stress-stretch curve that the IVD tissue displays stiffening behavior in compression. This trend was observed in the other studies examining the IVD under uniaxial compression [1,6]. Yahyaiee et al. [15] compared several hyperelastic models for the IVD tissue under physiological loads. The results of their finite element simulation revealed that the Yeoh model had the best consistency with the experimental data. This finding was also reported by Martins et al. [12]. On the other hand, the Neo-Hookean expression, which was the only single-parameter model, failed to properly fit the experimental data in comparison with other models, which was again consistent with the study of Yahyaiee et al. [15] and Martins et al. [12].

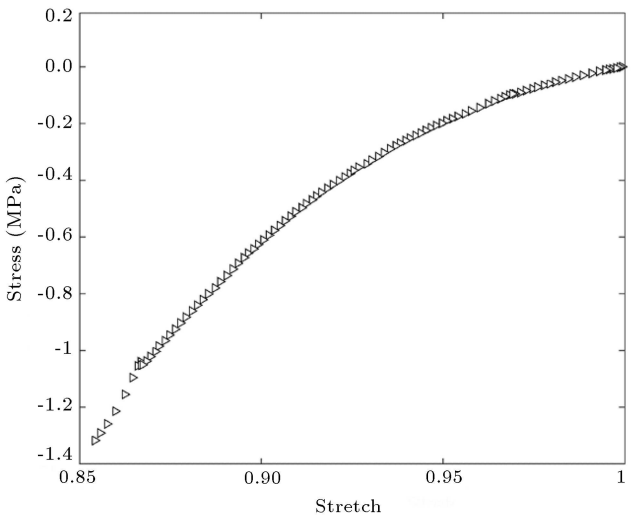

Figure 7. Mean Cauchy stress versus the mean stretch (λ) data obtained from the constant strain rate experiment.

In this study, several hyperelastic models were fitted to the mean stress-strain curve from the experimental data. The suitability of the fit is quantified by the values of the coefficient of determination, R^2, which were calculated for each fitting model. The best model for the hyperelastic behavior of the IVD tissue was selected based on the R^2 values. Table 8 lists the resultant R^2 values and the calculated parameters of each hyperelastic model. Yeoh, Mooney-Rivlin, and Ogden models had the closest R^2 values to 1.00, respectively.

Figure 8 exhibits the experimental data and the fitted curves of the models with stress functions in terms of stretches, i.e., Mooney-Rivlin, Ogden, and Neo-Hookean. It is apparent that the Neo-Hookean expression, which was the only single-parameter model, failed to properly fit the experimental data in comparison with other models, which was consistent with the study of Yahyaiee et al. [15] and Martins et al. [12]. In Figure 9, models with stress functions dependent on both the stretches and the first invariants (Yeoh, Veronda-Westmann, Fung, and Humphrey) are shown. Also, the residue of each model's prediction with the experimental data can be observed. Based on Figure 9, Fung and Humphrey's models yielded the same plots and R^2 values. In this group, the Yeoh model could best describe the hyperelastic response of the IVD tissue, consistent with the studies of Yahyaiee et al. [15] and Martins et al. [12].

The results of this part can be helpful to those seeking the best-describing models for IVD. Additionally, our findings provide future researchers with the mechanical parameters needed in the tissue models and simulations. This study can be taken up by

Table 8. R^2 values and the calculated parameters of the hyperelastic models used in this study.

Model	R^2	C_1	C_2	C_3	C_4	C_5	C_6
Mooney-Rivlin	0.9992	−0.01333	0.01385	–	–	–	–
Yeoh	0.9993	0.0005331	0.008229	−0.01575	–	–	–
Fung	0.9966	0.001363	11.43	–	–	–	–
Neo-Hookean	0.8967	0.001129	–	–	–	–	–
Humphrey	0.9966	5.959e-05	11.43	–	–	–	–
Ogden	0.9990	3.76	0.08065	3.483	0.07991	−2.085	0.2784
Veronda-Westmann	0.997	0.000185	7.439	–	–	–	–

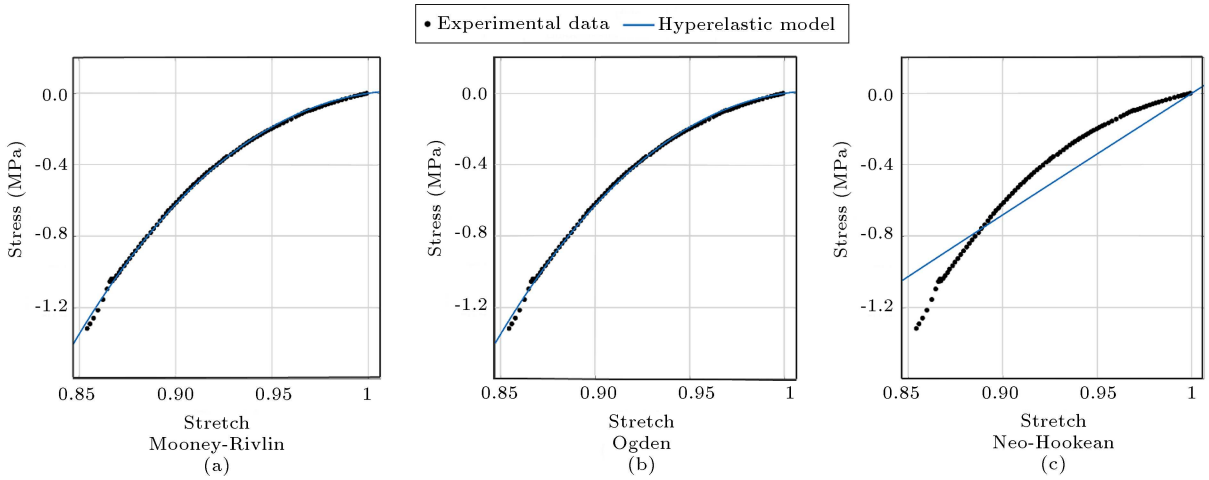

Figure 8. (a) Mooney-Rivlin, (b) Ogden, and (c) Neo-Hookean hyperelastic models fitted to the experimental data.

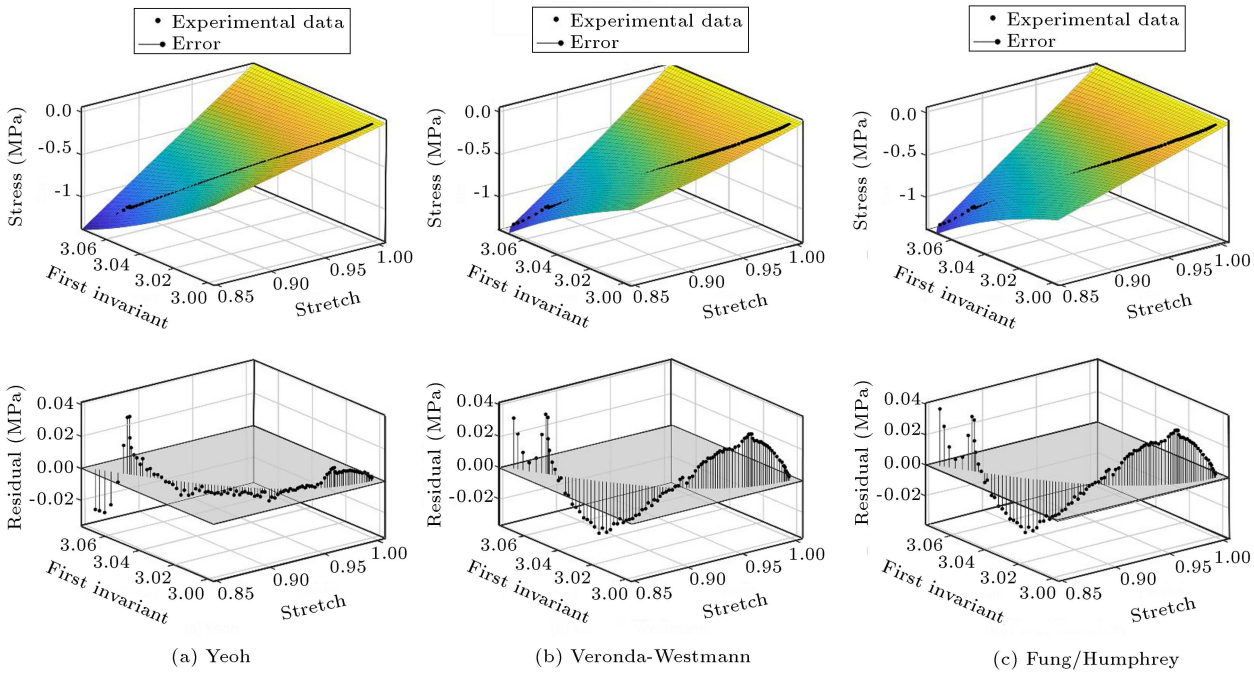

Figure 9. (a) Yeoh, (b) Veronda-Westmann, and (c) Fung and Humphrey hyperelastic models fitted to the experimental data.

researchers who need to have a properly characterized model, either hyperelastic or viscoelastic, based on the nature of their research. Future investigations can combine the best-fitting models in each group (Yeoh's hyperelastic model and MSP nonlinear viscoelastic model, for example) and study the hyper-viscoelastic behavior of the IVD.

4. Conclusion

In this study, ten samples of ovine cervical Intervertebral Discs (IVDs) were subjected to uniaxial compression to characterize the mechanical properties of this tissue. Relaxation tests with three different strain levels were performed on the samples. Three viscoelastic constitutive models with linear, quasi-linear, and nonlinear behavior were fitted to the mean Cauchy stress-time data from the experiments. In addition, a compressive load with a constant strain rate was applied to the IVD tissue samples for hyperelastic modeling. The mean Cauchy stress against the corresponding strain data was obtained and fitted by seven hyperelastic constitutive models, assuming isotropy and incompressibility of the tissue. The parameters of all the hyperelastic and viscoelastic models in this study were calculated and reported. Our findings can add to a growing body of literature on IVD mechanical characterization and shed light on the tissue's nonlinear

behavior. This study has led us to conclude the following:

- The MSP model, featuring a time- and strain-dependent relaxation function, was the most accurate model to obtain the viscoelastic response of the IVD at different strain levels;
- The Quasi-Linear Viscoelastic (QLV) model could predict the overall viscoelastic behavior of the IVD at different strain levels with acceptable accuracy;
- Linear viscoelastic models intrinsically fail to predict the IVD response at different strain levels. Thus, it was approved that the IVD viscoelastic behavior is not linear and must be delivered by a nonlinear model described here or in the literature;
- Yeoh, Mooney-Rivlin, and Ogden's models could fit the experimental data with the highest quality and, hence, best describe the hyperelastic behavior of the IVD tissue.

Acknowledgment

The authors acknowledge Professor Mehran Kasra and the Department of Biomedical Engineering of the Amirkabir University of Technology for providing the samples and assistance in the experimental facilities and setups. We extend our gratitude towards Professor Mohammad Tafazzoli-Shadpour for his advice and guidance. We would also like to thank all the students who aided in performing the experimental tests and measurements.

Funding

This research did not receive any specific grant from funding agencies in the public, commercial, or not-for-profit sectors.

Conflicts of interest statement

The authors confirm that this manuscript and its corresponding research work involves no.

Nomenclature

$A(\varepsilon)$	Strain-dependent parameter of the relaxation function in MSP model
$B(\varepsilon)$	Strain-dependent exponent of the relaxation function in MSP model
C	Right Cauchy-Green deformation tensor
C_i	Constant parameters of stress functions for hyperelastic material models
C_{ijk}	Constant parameters of Rivlin strain energy density function
dx	Material element at the new configuration (mm)
dx_i	Material element at the new configuration in x_1 direction (mm)
dX	Material element at the reference configuration (mm)
dX_i	Material element at the reference configuration in x_1 direction (mm)
E	Spring stiffness (MPa)
E_0	Spring stiffness of the Maxwell arm in the standard linear solid model (MPa)
E_1	Stiffness of spring 1 in the standard linear solid model (MPa)
E_2	Stiffness of spring 2 in the standard linear solid model (MPa)
E_i	Stiffness parameter of the standard linear solid model (MPa)
$E(t)$	Relaxation function (MPa)
F	Deformation gradient tensor
$G(\varepsilon)$	Strain-dependent parameter of the separable relaxation function in the QLV model
I_1	First invariant of the right Cauchy-Green deformation tensor
I_2	Second invariant of the right Cauchy-Green deformation tensor
I_3	Third invariant of the right Cauchy-Green deformation tensor
J	Determinant of the deformation gradient tensor
n	Rate of relaxation
P	Hydrostatic pressure (MPa)
R^2	Coefficient of determination (R-squared)
t	Time (s)
$T(t)$	Time-dependent parameter of the separable relaxation function in the QLV model
W	Strain energy density function (MPa)
ε	Strain
ε_0	Constant strain input
$\varepsilon(t)$	Strain function
η	Dashpot viscosity (MPa.s)
λ	Principal stretch in the x_1 direction
λ_i	Principal stretches in the x_i direction
σ	Stress (MPa)
σ_i	Cauchy stress tensor (MPa)
$\sigma(t)$	Stress response as a function of time (MPa)

τ	Time variable of Boltzmann superposition integral (s)
τ_1	Relaxation time parameter of spring 1 and dashpot 1 (s)
τ_2	Relaxation time parameter of spring 2 and dashpot 2 (s)
τ_i	Relaxation time parameters (s)
τ_r	Relaxation time (s)

References

1. Ghezelbash, F., Shirazi-Adl, A., Baghani, M., et al. "On the modeling of human intervertebral disc annulus fibrosus: Elastic, permanent deformation and failure responses", *Journal of Biomechanics*, **102**, 109463 (2020).
https://doi.org/10.1016/j.jbiomech.2019.109463
2. Ogden, R.W., *Non-linear Elastic Deformations*, Courier Corporation (1997).
3. Komeili, A., Rasoulian, A., Moghaddam, F., et al. "The importance of intervertebral disc material model on the prediction of mechanical function of the cervical spine", *BMC Musculoskeletal Disorders*, **22**(1), p. 324 (2021).
DOI: 10.1186/s12891-021-04172-1
4. Jafari, B., Katoozian, H.R., Tahani, M., et al. "A comparative study of bone remodeling around hydroxyapatite-coated and novel radial functionally graded dental implants using finite element simulation", *Medical Engineering and Physics*, **102**, 103775 (2022).
DOI: 10.1016/j.medengphy.2022.103775
5. Sadeghnejad, S., Elyasi, N., Farahmand, F., et al. "Hyperelastic modeling of sino-nasal tissue for haptic neurosurgery simulation", *Scientia Iranica*, **27**(3), pp. 1266–1276 (2020).
DOI: 10.24200/SCI.2019.50348.1652
6. Casaroli, G., Galbusera, F., Jonas, R., et al. "A novel finite element model of the ovine lumbar intervertebral disc with anisotropic hyperelastic material properties", *PLoS One*, **12**(5), 0177088 (2017).
DOI: 10.1371/journal.pone.0177088
7. Kandziora, F., Pflugmacher, R., Scholz, M., et al. "Comparison between sheep and human cervical spines: an anatomic, radiographic, bone mineral density, and biomechanical study", *Spine*, **26**(9), pp. 1028–1037 (2001).
DOI: 10.1097/00007632-200105010-00008
8. Valentin, S. and Licka, T.F. "Spinal motion and muscle activity during active trunk movements-comparing sheep and humans adopting upright and quadrupedal postures", *Plos One*, **11**(1), 0146362 (2016).
DOI: 10.1371/journal.pone.0146362
9. Qiu, T.-X., Tan, K.-W., Lee, V.-S., et al. "Investigation of thoracolumbar T12-L1 burst fracture mechanism using finite element method", *Medical Engineering and Physics*, **28**(7), pp. 656–664 (2006).
DOI: 10.1016/j.medengphy.2005.10.011
10. Yang, H., Jekir, M.G., Davis, M.W., et al. "Effective modulus of the human intervertebral disc and its effect on vertebral bone stress", *Journal of Biomechanics*, **49**(7), pp. 1134–1140 (2016).
DOI: 10.1016/j.jbiomech.2016.02.045
11. Green, T., Adams, M., and Dolan, P. "Tensile properties of the annulus fibrosus", *European Spine Journal*, **2**(4), pp. 209–214 (1993).
DOI: 10.1007/BF00299447
12. Martins, P., Natal Jorge, R., and Ferreira, A. "A comparative study of several material models for prediction of hyperelastic properties: Application to silicone-rubber and soft tissues", *Strain*, **42**(3), pp. 135–147 (2006).
DOI: 10.1111/j.1475-1305.2006.00257.x
13. Wagnac, E., Arnoux, P.-J., Garo, A., et al. "Calibration of hyperelastic material properties of the human lumbar intervertebral disc under fast dynamic compressive loads", *Journal of Biomechanical Engineering*, **133**(10), 101007-1–101007-10 (2011).
DOI: 10.1115/1.4005224
14. Newell, N., Carpanen, D., Grigoriadis, G., et al. "Material properties of human lumbar intervertebral discs across strain rates", *The Spine Journal*, **19**(12), pp. 2013–2024 (2019).
DOI: 10.1016/j.spinee.2019.07.012
15. Yahyaiee, A., Karimi, A., and Rouhi, G. "Comparison of four hyperelastic models for intervertebral discs: A finite element study", *28th Annual International Conference of Iranian Society of Mechanical Engineering (ISME2020)*, Tehran, Iran (2020).
16. Safshekan, F., Tafazzoli-Shadpour, M., Abdouss, M. and Shadmehr, M.B. "Viscoelastic properties of human tracheal tissues", *Journal of Biomechanical Engineering*, **139**(1), 011007 (2017).
https://doi.org/10.1186/s12931-017-0540-y
17. Ekström, L., Kaigle, A., Hult, E., et al. "Intervertebral disc response to cyclic loading-an animal model", *Proceedings of the Institution of Mechanical Engineers, Part H: Journal of Engineering in Medicine*, **210**(4), pp. 249–258 (1996).
DOI: 10.1243/PIME_PROC_1996_210_421_02
18. Ellingson, A.M. and Nuckley, D.J. "Intervertebral disc viscoelastic parameters and residual mechanics spatially quantified using a hybrid confined/in situ indentation method", *Journal of Biomechanics*, **45**(3), pp. 491–496 (2012).
DOI: 10.1016/j.jbiomech.2011.11.050
19. Groth, K.M. and Granata, K.P. "The viscoelastic standard nonlinear solid model: Predicting the response of the lumbar intervertebral disk to low-frequency vibrations", *Journal of Biomechanical Engineering*, **130**(3), 031005-1–031005-6 (2008).
DOI: 10.1115/1.2904464

20. Yoganandan, N., Umale, S., Stemper, B., et al. "Fatigue responses of the human cervical spine intervertebral discs", *Journal of the Mechanical Behavior of Biomedical Materials*, **69**, pp. 30–38 (2017). https://doi.org/10.1016/j.jmbbm.2016.11.026

21. Lakes, R.S., *Viscoelastic Solids*, 9 CRC Press (1998).

22. Provenzano, P., Lakes, R., Corr, D., et al. "Application of nonlinear viscoelastic models to describe ligament behavior", *Biomechanics and Modeling in Mechanobiology*, **1**(1), pp. 45–57 (2002). DOI: 10.1007/s10237-002-0004-1

23. Sciortino, V., Cerniglia, D., Pasta, S., et al., *Fractional Calculus as a New Perspective in the Viscoelastic Behaviour of the Intervertebral Disc*, European Workshop on Structural Health Monitoring, pp. 915–925 (2023). https://doi.org/10.1007/978-3-031-07254-3-92

24. Jafari, B., Shams, V., Esfandiari, M., et al. "Nonlinear contact modeling and haptic characterization of the ovine cervical intervertebral disc", *2022 9th IEEE RAS/EMBS International Conference for Biomedical Robotics and Biomechatronics (BioRob)*, Seoul, South Korea, pp. 1–6 (2022). DOI: 10.1109/BioRob52689.2022.9925398

25. Newell, N., Little, J., Christou, A., et al. "Biomechanics of the human intervertebral disc: A review of testing techniques and results", *Journal of the Mechanical Behavior of Biomedical Materials*, **69**, pp. 420–434 (2017). https://doi.org/10.1016/j.jmbbm.2017.01.037

26. Kasra, M., Parnianpour, M., Shirazi-Adl, A., et al. "Effect of strain rate on tensile properties of sheep disc anulus fibrosus", *Technology and Health Care*, **12**(4), pp. 333–342 (2004). DOI: 10.3233/THC-2004-12405

27. Fung, Y.-C., *Biomechanics: Mechanical Properties of Living Tissues*, Springer Science and Business Media (2013).

28. Darijani, H. and Naghdabadi, R. "Hyperelastic materials behavior modeling using consistent strain energy density functions", *Acta Mechanica*, **213**(3–4), pp. 235–254 (2010). DOI: 10.1007/s00707-009-0239-3

29. Safshekan, F., Tafazzoli-Shadpour, M., Abdouss, M., et al. "Mechanical characterization and constitutive modeling of human trachea: age and gender dependency", *Materials*, **9**(6), p. 456 (2016). DOI: 10.3390/ma9060456

30. Sadeghnejad, S., Esfandiari, M., Farahmand, F., et al. "Phenomenological contact model characterization and haptic simulation of an endoscopic sinus and skull base surgery virtual system", *4th International Conference on Robotics and Mechatronics (ICROM)*, (IEEE), pp. 84–89 (2016). DOI: 10.1109/ICRoM.2016.7886822

Biographies

Bahram Jafari obtained his BS degree in Mechanical Engineering from Ferdowsi University of Mashhad (FUM), Mashhad, Iran in 2018, and his MS degree in Biomedical Engineering-Biomechanics from Amirkabir University of Technology (Tehran Polytechnic), Tehran, Iran in 2021. He is, currently, a PhD student of Biomedical Engineering, and is studying a joint program at the University of Texas at San Antonio (UTSA) and the University of Texas Health Science Center at San Antonio (UTHSCSA). His activities and research interests are related to the mechanical modeling of hard and soft tissues and the simulation of the brain and related biological processes.

Vida Shams Esfand Abadi obtained her BS degree in Electrical Engineering from University of Shahrekord, Chaharmahal va Bakhtiari, Iran in 2013 and her MS degree in Robotic Engineering-from Amirkabir University of Technology (Tehran Polytechnic), Tehran, Iran in 2017. She is, currently, a PhD student of Biomedical Engineering, and is studying the biomechanics of gait at the Amirkabir University of Technology since 2018. Her activities and research interests are related to modeling of soft tissue balancing in Total Knee Arthroplasty (TKA) and related biomechanical processes.

Soroush Sadeghnejad is an Assistant Professor in the Department of Biomedical Engineering at the Amirkabir University of Technology, Tehran, Iran since 2020. He is also the director of The Bio-Inspired System Design Laboratory, active in the field of medical and rehabilitation robotics. Dr. Sadeghnejad's research interests broadly involve the areas of medical and rehabilitation robotics and systems control. Specifically, his research focuses on haptics and teleoperation control, medical robotics, and robot-assisted interventions. Dr. Sadeghnejad is currently the vice-president of the International Robot Sport Association (FIRA).